

# Electronic Phase Diagram of High- $T_c$ Cuprate Superconductors from a Mapping of the In-Plane Resistivity Curvature

Yoichi Ando,\* Seiki Komiya, Kouji Segawa, S. Ono, and Y. Kurita  
Central Research Institute of Electric Power Industry, Komae, Tokyo 201-8511, Japan.  
(Dated: July 26, 2021)

We propose that Resistivity Curvature Mapping (RCM) based on the in-plane resistivity data is a useful way to objectively draw an electronic phase diagrams of high- $T_c$  cuprates, where various *crossovers* are important. In particular, the pseudogap crossover line can be conveniently determined by RCM. We show experimental phase diagrams obtained by RCM for  $\text{Bi}_2\text{Sr}_{2-z}\text{La}_z\text{CuO}_{6+\delta}$ ,  $\text{La}_{2-x}\text{Sr}_x\text{CuO}_4$ , and  $\text{YBa}_2\text{Cu}_3\text{O}_y$ , and demonstrate the universal nature of the pseudogap crossover. Intriguingly, the electronic crossover near optimum doping depicted by RCM appears to occur rather abruptly, suggesting that the quantum critical regime, if exists, must be very narrow.

PACS numbers: 74.25.Fy, 74.25.Dw, 74.72.Hs, 74.72.Dn, 74.72.Bk

Elucidating the electronic phase diagram of high- $T_c$  cuprates in the temperature ( $T$ ) vs doping ( $p$ ) plane is an important experimental step towards understanding the high- $T_c$  superconductivity. When there is a clear phase transition, such as the superconducting transition or the Néel transition, it is easy to locate the transition line in the  $T$  vs  $p$  plane. However, when there is a *crossover* in the electronic properties, it becomes non-trivial to define the crossover and to locate the crossover line. In the case of cuprates, there is an important crossover line in the phase diagram, that is, the crossover to the pseudogap phase within the normal state [1, 2]; also, there is another putative crossover from a non-Fermi liquid to a Fermi liquid in the overdoped regime [2]. Because of the lack of a universal and objective way to determine these crossover lines, the phase diagram of the cuprates has been rather loosely discussed in the past [2, 3, 4, 5] and it is not known to what extent the putative phase diagram is generic.

In this Letter, we propose a novel way to objectively draw the  $T$  vs  $p$  phase diagram based on the in-plane resistivity ( $\rho_{ab}$ ) data. We call this new method “Resistivity Curvature Mapping” (RCM), because the curvature (second derivative) of the  $\rho_{ab}(T)$  data is mapped onto the  $T$  vs  $p$  plane, graphically showing how the behavior of  $\rho_{ab}$  changes as a function of temperature and doping reflecting the changes in the underlying electronic phase. The actual phase diagrams obtained by RCM are presented for three hole-doped cuprates,  $\text{Bi}_2\text{Sr}_{2-z}\text{La}_z\text{CuO}_{6+\delta}$  (BSLCO),  $\text{La}_{2-x}\text{Sr}_x\text{CuO}_4$  (LSCO), and  $\text{YBa}_2\text{Cu}_3\text{O}_y$  (YBCO), in all of which the hole doping can be widely changed from underdoped to overdoped regimes. The phase diagrams of the three systems demonstrate that the pseudogap crossover line, which can be conveniently determined by RCM, shows a linear doping dependence (in the superconducting doping regime) and is terminated near optimum doping. Furthermore, our data demonstrate that the well-known “ $T$ -linear” resistivity is observed in a very limited region of the phase diagram near optimum doping, which suggests that the

quantum-critical non-Fermi-liquid regime [2], if exists, must be much narrower than is often conjectured [2, 6].

The single crystals of BSLCO, LSCO, and YBCO are grown by a floating-zone technique [7], a traveling-solvent floating-zone technique [8], and a flux method [9], respectively. For BSLCO, we first determined the actual La content,  $z$ , of representative samples by the inductively-coupled plasma atomic-emission spectroscopy (ICP-AES) and established a relationship between  $z$  and the  $c$ -axis lattice constant  $c_0$ ; we then measure  $c_0$  of all the samples to determine actual  $z$ . Since the relation between  $z$  and  $p$  (hole doping per Cu) has been sorted out in our previous study [10], here we show just the  $p$  values for our BSLCO samples for simplicity. In the case of LSCO, one can safely assume that the  $p$  value is equal to  $x$  (Sr content), as long as the samples are carefully annealed to remove excess oxygen or oxygen vacancies, which is what we always do for our LSCO crystals [8]. On the other hand, it is difficult to determine the exact hole doping  $p$  in the  $\text{CuO}_2$  planes of YBCO [11], so here we just show the oxygen content  $y$ , which is measured by iodometry and is the control parameter of the doping. We have established a technique to reliably and reproducibly anneal the YBCO crystals to tune  $y$  to a target value [9]; we always quench the sample to room temperature at the end of the annealing to avoid the long-range oxygen ordering phenomena, which often complicate the physics of YBCO [12]. Our previous study indicated that the hole doping  $p$  changes smoothly with  $y$  (without showing a plateau near  $y \sim 6.6$ ) in our quenched samples [9, 11]. All the YBCO samples are untwinned crystals and the  $a$ -axis resistivity  $\rho_a$  is measured to avoid direct contributions from the  $\text{CuO}$  chains, which run along the  $b$ -axis. The resistivity is measured with a standard ac four-probe technique [13].

Figure 1(a) shows the  $\rho_{ab}(T)$  data of BSLCO for  $p = 0.11 - 0.18$  at 0.01 intervals; note that optimum doping of this system corresponds to  $p = 0.16$  where the zero-resistivity  $T_c$  is 36–38 K [10, 14]. To compare the  $\rho_{ab}(T)$  behavior for different dopings, we normalize  $\rho_{ab}$

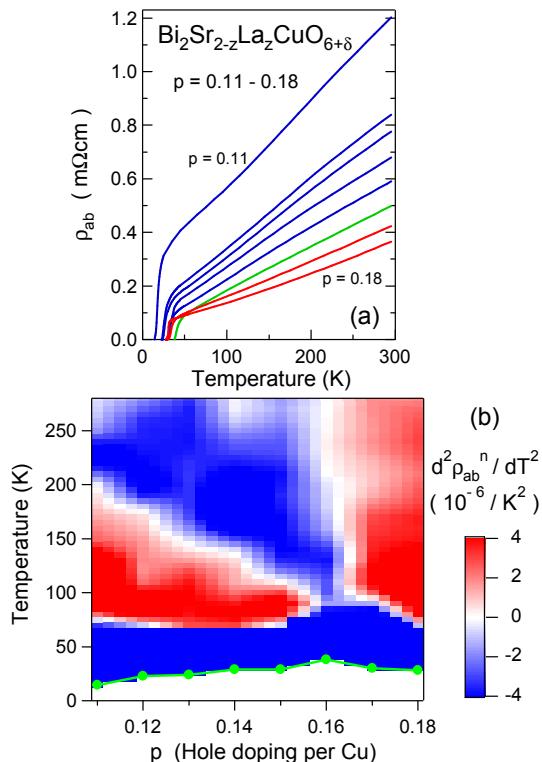


FIG. 1: (a)  $\rho_{ab}(T)$  data of BSLCO for  $p = 0.11$ – $0.18$  at  $0.01$  intervals; the data for underdoped (overdoped) samples are shown in blue (red), while that for optimum doping is shown in green. (b) Resistivity curvature mapping, namely, a false color mapping of  $d^2\rho_{ab}^n/dT^2$  in the  $T$  vs  $p$  plane, for BSLCO. The solid green circles show  $T_c$ 's for the measured compositions.

by its 300-K value to obtain  $\rho_{ab}^n [= \rho_{ab}/\rho_{ab}(300\text{K})]$ . By calculating the second derivative of  $\rho_{ab}^n(T)$ ,  $d^2\rho_{ab}^n/dT^2$ , for each doping (wherein we employ modest numerical smoothing [15]) and linearly interpolating the results, we can draw a false color mapping of  $d^2\rho_{ab}^n/dT^2$  in the  $T$  vs  $p$  plane as shown in Fig. 1(b), where the red (blue) color corresponds to positive (negative) curvature, while the white color means that the curvature is essentially zero. Note that when  $\rho_{ab}(T)$  changes linearly with  $T$ , the curvature of  $\rho_{ab}(T)$  is zero; thus, the vertical white band apparent in Fig. 1(b) at  $p \simeq 0.16$  means that the  $T$ -linear resistivity is observed there. Furthermore, the vertical red region in Fig. 1(b) for  $p \gtrsim 0.17$  graphically demonstrates that as soon as BSLCO is overdoped the  $\rho_{ab}(T)$  behavior loses the  $T$ -linearity; actually, we have shown [16] that  $\rho_{ab}(T)$  of the overdoped BSLCO samples are well fitted with  $\sim T^\alpha$  with  $\alpha > 1$ .

More importantly, Fig. 1(b) also depicts the effect of the pseudogap opening in underdoped samples: It is known [16, 17] that the pseudogap tends to cause  $\rho_{ab}(T)$  to show an ‘‘S-shape’’ behavior, which has been interpreted to be due to a rapid reduction in the inelastic scattering rate of the electrons in the pseudogap phase

upon lowering temperature [17]. Although it was recently proposed [18] that this S-shape may better be viewed in terms of a gradual participation of the quasiparticles near  $(\pi, 0)$  of the Brillouin zone with increasing temperature, in any case the partial destruction of the Fermi surface [19] is responsible for the peculiar  $\rho_{ab}(T)$  behavior in the pseudogap phase. If one accepts the S-shape to be a signature of the pseudogap in the dc transport, then there is a unique and unambiguous temperature which characterizes the S-shape, that is, the inflection point. It is thus natural to consider the inflection point in the  $\rho_{ab}(T)$  curve as a ‘‘characteristic temperature’’ of the pseudogap,  $T_{pg}$ , though it may not denote the ‘‘onset’’ of the pseudogap. In our RCM the inflection point shows up in white, so the diagonal white band that vertically separates the blue and red regions in the underdoped regime ( $p < 0.16$ ) signifies how the characteristic temperature for the pseudogap crossover changes with doping. It is intriguing to see that the pseudogap boundary signified by  $T_{pg}$  changes essentially linearly with doping and is terminated near optimum doping.

In the literature, the pseudogap temperature  $T^*$  has often been extracted from the  $\rho_{ab}(T)$  data by identifying the temperature below which  $\rho_{ab}$  deviates downwardly from the high-temperature  $T$ -linear behavior [17, 20]. However, there are two major shortcomings in this approach. First, in many cases there is not a wide-enough temperature range where the ‘‘high-temperature  $T$ -linear behavior’’ is unambiguously determined; in fact, our data in Fig. 1(b) demonstrate that there is no well-defined  $T$ -linear region at high temperature (which should identify itself as a horizontal white band at the top of the diagram) in underdoped BSLCO. Second, it is difficult to objectively identify a ‘‘deviation point’’ when the deviation occurs gradually and continuously. These shortcomings have been part of the reasons why  $T^*$  has been only loosely discussed and its generic behavior is not agreed upon. Furthermore, since the paraconductivity due to the superconducting fluctuations (SCF) also reduces  $\rho_{ab}$  and leads to a negative curvature in  $\rho_{ab}(T)$ , it is sometimes difficult to judge whether the deviation from the high-temperature  $T$ -linear behavior is due to the pseudogap or the SCF, particularly when the SCF can start from quite a high temperature [21]. [In Fig. 1(b), the blue region immediately above  $T_c$  is where the SCF is dominant.] An obvious merit of the present definition of  $T_{pg}$  is that those ambiguities can naturally be avoided.

Next we discuss LSCO, for which the raw  $\rho_{ab}(T)$  data are shown in Figs. 2(a-b). For clarity, we use the nominal  $x$  values for the LSCO samples here, but we confirmed that the actual Sr contents measured by ICP-AES agree with the nominal  $x$  values within an error of less than 5%. The RCM plot for LSCO [Fig. 2(c)] is a bit complicated due to the existence of the structural phase transition from the high-temperature tetragonal phase to the low-temperature orthorhombic phase, which causes a weak

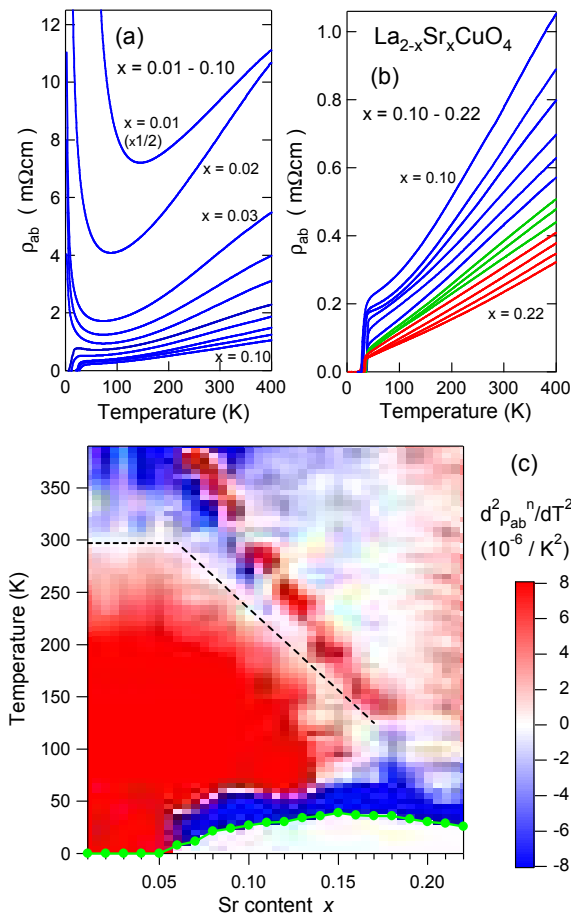


FIG. 2: (a,b)  $\rho_{ab}(T)$  data of LSCO for  $x = 0.01$ – $0.22$  at  $0.01$  intervals. (c) Electronic phase diagram depicted by RCM for LSCO; here  $\rho_{ab}^n = \rho_{ab} / \rho_{ab}(400K)$ . The dashed line is a guide to the eyes to emphasize  $T_{pg}$  and the solid green circles show  $T_c$ 's for the measured compositions.

kink in the  $\rho_{ab}(T)$  data; the diagonal red band that ends at  $x = 0.18$  signifies this transition, whose position is consistent with the data in the literature [22]. Apart from this structural transition, one can see that the phase diagram of LSCO depicted by RCM is very similar to that of BSLCO in several respects: First, the  $T$ -linear resistivity (vertical white band) is observed only near optimum doping ( $x \approx 0.16 - 0.18$ ). Second, the vertical red region for  $p \gtrsim 0.19$  demonstrates that the  $\rho_{ab}(T)$  behavior becomes positively curved in the overdoped regime. Third,  $T_{pg}$  (marked by a dashed line) changes approximately linearly with  $x$  for  $x \geq 0.06$  and is terminated near optimum doping; incidentally, it is intriguing to see that  $T_{pg}$  saturates in the non-superconducting regime ( $x < 0.06$ ) and that the saturated value of  $T_{pg}$  is close to the Néel temperature for  $x = 0$  ( $\sim 300$  K) [22].

Figures 3(a-b) show the  $\rho_a(T)$  data for YBCO, and the RCM plot is shown in Fig. 3(c). One can easily see that the phase diagram of YBCO depicted in Fig. 3(c) is quite similar to those of BSLCO and LSCO in that (1) the  $T$ -

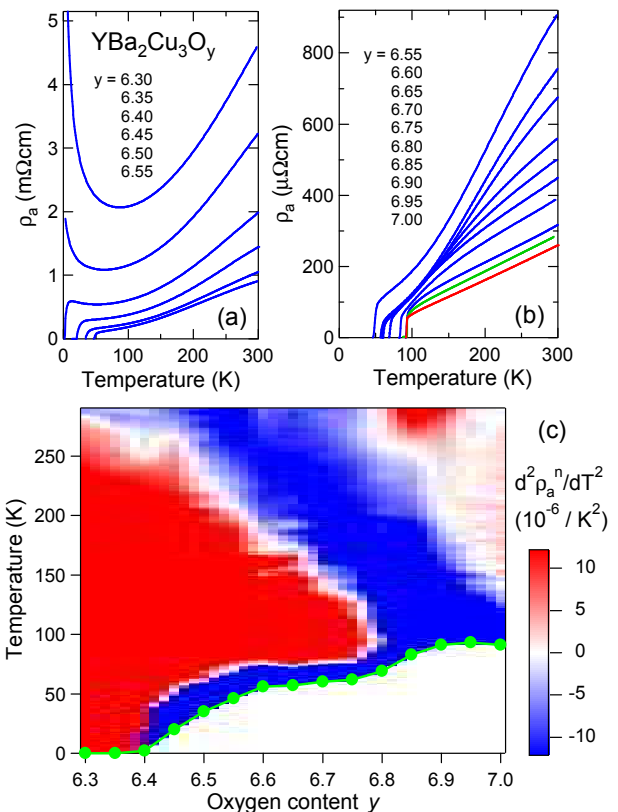


FIG. 3: (a,b)  $\rho_a(T)$  data of YBCO for  $y = 6.30$ – $7.00$  at  $0.05$  intervals. (c) Electronic phase diagram depicted by RCM for YBCO, where the solid green circles show  $T_c$ 's for the measured compositions.

linear resistivity is observed only near optimum doping (*i.e.*,  $y \approx 6.95$ ), and (2)  $T_{pg}$  changes approximately linearly with  $y$  in the superconducting regime and tends to saturate in the antiferromagnetic regime. In addition, one can see that  $\rho_a(T)$  becomes slightly positively curved in the overdoped regime, which is recognized by the faint red color at  $y = 7.00$  for  $T > 150$  K. However, Fig. 3(c) also shows a departure from the universal phase diagram suggested by BSLCO and LSCO in two aspects: (1)  $T_{pg}$  is terminated at  $y \approx 6.8$ , which is near optimum doping but is in the underdoped regime, and (2) the high-temperature behavior at  $6.80 \lesssim y \lesssim 6.90$  is complicated. (The red blob at the top of the diagram for  $6.85 \leq y \leq 6.90$  is due to a slight curving of the  $\rho_a(T)$  data near 300 K at these dopings, which we confirm to be very reproducible; this is due to the oxygen motion in the Cu-O chains [23].) Phenomenologically, it appears that these peculiarities are related to the fact that the  $T_c$ -vs- $y$  diagram of YBCO [see the green symbols in Fig. 3(c)] shows two plateaus at  $\sim 60$  K and  $\sim 90$  K, the former called the 60-K phase and its origin is still under debate [9]; clearly, the phase diagram is more ordinary in the 60-K phase and below ( $y \leq 6.80$ ), but becomes peculiar near the 90-K phase. One interesting possibility is that

the phase diagram for  $y \leq 6.80$  reflects the physics of the  $\text{CuO}_2$  planes alone, while in the 90-K phase the Cu-O chains introduce additional complications. In any case, the slight nonuniversality in YBCO is most likely related to its structural peculiarity.

The above results demonstrate that the cuprate phase diagram is surprisingly universal unless some additional feature (such as the Cu-O chains in YBCO) adds another layer of complications. In particular, the fact that the  $T$ -linear resistivity is observed only near optimum doping and  $\rho_{ab}(T)$  becomes positively curved as soon as the system is overdoped is commonly observed in the three cuprate systems studied here. In this regard, our data do not give strong support to the notion that the  $T$ -linear resistivity is associated with a quantum critical region (where the physics is scaled by a single energy scale  $T$  [6]); based on our data, one should probably conclude that the quantum critical region, if exists, must be much narrower in cuprates than is observed in other systems [24, 25], where it clearly fans out with increasing  $T$  like an inverse triangle. It seems that our data (particularly those of BSLCO) would rather suggest that there are simply two different electronic states for underdoped and overdoped regimes, and the  $T$ -linear resistivity appears to be a property of a singular electronic state realized only at optimum doping. It is useful to note that such an abrupt nature of the crossover at optimum doping might be related to a change in the underlying Fermi-surface state, which was recently shown to occur at optimum doping in BSLCO [26].

Finally, it is useful to note that in all three cuprates the pseudogap crossover line  $T_{pg}(p)$  is terminated somewhere near optimum doping and it does not extend into the overdoped regime. This might appear to be inconsistent with the results of the angle-resolved photoemission spectroscopy (ARPES) [27] or the scanning tunneling microscope (STM) [28] that observed a pseudogap in overdoped samples, but such apparent inconsistency is probably a manifestation of the fact that the pseudogap in the cuprates has two different origins [29, 30] and only one of them is responsible for the S-shape in  $\rho_{ab}(T)$ . In this regard, it is useful to note that the SCF are probably related to various pseudogap features that occur rather close to  $T_c$  [29, 30, 31], and in this sense the blue region immediately above  $T_c$  in our RCM plots can be considered to be representative of the pseudogap of a different origin; this interpretation is actually consistent with the phase diagram of BSLCO depicted by the  $c$ -axis magnetoresistance [29]. In passing, we note that the pseudogap is known to be most directly probed in the  $c$ -axis properties [1, 2, 29] and  $T_{pg}$  determined here from RCM is rather indirectly reflecting the pseudogap, probably giving a lower measure of its development.

In summary, we demonstrate that the Resistivity Curvature Mapping (RCM) offers a powerful tool to draw an electronic phase diagram of high- $T_c$  cuprates based on the

resistivity data. The biggest merit of this method is that it allows one to objectively draw the pseudogap crossover line  $T_{pg}(p)$ . It also allows one to see where in the phase diagram the  $T$ -linear resistivity is observed. The RCM-derived phase diagrams we present for BSLCO, LSCO, and YBCO demonstrate that the essential feature of the phase diagram is surprisingly universal and that the electronic crossover near optimum doping occurs rather abruptly.

We thank A. N. Lavrov for helpful discussions.

---

\* Electronic address: ando@criepi.denken.or.jp

- [1] T. Timusk and B. Statt, Rep. Prog. Phys. **62**, 61 (1999).
- [2] J. Orenstein and A. J. Millis, Science **288**, 468 (2000).
- [3] P. W. Anderson, Science **288**, 480 (2000).
- [4] B. Batlogg and V. J. Emery, Nature **382**, 20 (1996).
- [5] E. W. Carlson, V. J. Emery, S. A. Kivelson, and D. Orgad, cond-mat/0206217.
- [6] S. Sachdev, Science **288**, 475 (2000).
- [7] S. Ono and Y. Ando, Phys. Rev. B **67**, 104512 (2003).
- [8] S. Komiya, Y. Ando, X. F. Sun, and A. N. Lavrov, Phys. Rev. B **65**, 214535 (2002).
- [9] K. Segawa and Y. Ando, Phys. Rev. Lett. **86**, 4907 (2001).
- [10] Y. Ando *et al.*, Phys. Rev. B **61**, R14956 (2000); **63**, 069902(E) (2001).
- [11] K. Segawa and Y. Ando, Phys. Rev. B **69**, 104521 (2004).
- [12] Y. Ando, K. Segawa, A. N. Lavrov, and S. Komiya, J. Low Temp. Phys. **131**, 793 (2003).
- [13] Y. Ando *et al.*, Phys. Rev. Lett. **87**, 017001 (2001).
- [14] S. Ono *et al.*, Phys. Rev. Lett. **85**, 638 (2000).
- [15] At each  $T$ , we fit the raw data in a window  $T \pm \Delta T$  with a polynomial of order 2 – 4 and take its second derivative ( $\Delta T$  is typically 5 K); the resulting RCM is essentially the same for  $\Delta T$  of 2 – 10 K, except that a sharp feature gets gradually smeared with increasing  $\Delta T$ .
- [16] Y. Ando and T. Murayama, Phys. Rev. B **60**, R6991 (1999).
- [17] T. Ito, K. Takenaka, and S. Uchida, Phys. Rev. Lett. **70**, 3995 (1993).
- [18] Y. Ando *et al.*, Phys. Rev. Lett. **92**, 197001 (2004).
- [19] M. R. Norman *et al.*, Nature **392**, 157 (1998).
- [20] T. Watanabe, T. Fujii, and A. Matsuda, Phys. Rev. Lett. **79**, 2113 (1997).
- [21] Y. Ando and K. Segawa, Phys. Rev. Lett. **88**, 167005 (2002).
- [22] M. A. Kastner, R. J. Birgeneau, G. Shirane, and Y. Endoh, Rev. Mod. Phys. **70**, 897 (1998).
- [23] A. N. Lavrov, Phys. Lett. A **168**, 71 (1992).
- [24] J. Custers *et al.*, Nature **424**, 524 (2003).
- [25] R. S. Perry *et al.*, Phys. Rev. Lett. **86**, 2661 (2001).
- [26] F. F. Balakirev *et al.*, Nature **424**, 912 (2003).
- [27] A. Damascelli, Z. Hussain, and Z.X. Shen, Rev. Mod. Phys. **75**, 473 (2003).
- [28] M. Kugler *et al.*, Phys. Rev. Lett. **86**, 4911 (2001).
- [29] A. N. Lavrov, Y. Ando, and S. Ono, Europhys. Lett. **57**, 267 (2002).
- [30] R. S. Markiewicz, Phys. Rev. Lett. **89**, 229703 (2002).
- [31] Y. Wang *et al.*, Phys. Rev. B **64**, 224519 (2001).